JOURNAL OF SOLID STATE CHEMISTRY 95, 1–13 (1991)

Neutron Diffraction Investigation of Magnetic Phase Transitions to Long-Range Antiferromagnetic Ordering in the "Free-Electron" Praseodymium Halides Pr_2X_5 (X = Br, I)

KARL KRÄMER AND GERD MEYER*

Institut für Anorganische Chemie, Universität Hannover, Callinstr. 9, W-3000 Hannover, Federal Republic of Germany

PETER FISCHER*

Labor für Neutronenstreuung, ETH Zürich, CH-5232 Villigen PSI, Switzerland

ALAN W. HEWAT

Institut Laue-Langevin, F-38042 Grenoble Cedex, France

AND HANS U. GÜDEL

Institut für Anorganische, Analytische, und Physikalische Chemie, Universität Bern, Freiestr. 3, CH-3000 Bern, Switzerland

Received February 13, 1991; in revised form June 10, 1991

Powder neutron and single-crystal X-ray diffraction experiments of the halides $Pr_2X_5 \triangleq (Pr^{3+})_2(X^-)_5(e^-)$ were performed in order to determine temperature dependences of the structure and to establish the nature of the magnetic phase transitions. Bulk magnetic measurements in the temperature range of 1.6 to 300 K showed remarkably high ordering temperatures. Pr_2Br_5 orders antiferromagnetically at T_N = 50(1) K, corresponding to the Shubnikov space group $P2_1/m'$, i.e., $\mathbf{k} = 0$. Below $T \approx 25$ K the ordered magnetic moments of the two inequivalent Pr^{3+} ions increase abruptly from $\mu_{Pr1} = 1.2\ \mu_B$ and $\mu_{Pr2} = 2.2\ \mu_B$ at 30 K to the saturation values $\mu_{Pr1} = 1.9\ \mu_B$ and $\mu_{Pr2} = 2.6\ \mu_B$. Below T_N = 37(1) K, Pr_2I_5 shows antiferromagnetic ordering corresponding to $\mathbf{k}$ = [1/2,0,0] and the Shubnikov space group P_a2_1 with ordered magnetic moments at saturation: $\mu_{Pr1} = 2.1\ \mu_B$ and $\mu_{Pr2} = 1.8\ \mu_B$. Measurements of average electrical conductivities of polycrystalline Pr_2X_5 indicate semiconducting behavior.

Introduction

Almost 30 years ago the praseodymium/praseodymium chloride, bromide, and iodide systems, M/MX_3, were investigated (*1–3*). In the course of such systematic investigations "line phases" like $PrBr_{2.38}$ and $PrI_{2.42}$ were observed and at that time only powder X-ray data could be obtained. In the meantime the crystal structure of Pr_2I_5 has been determined (*4*) and it seems clear that this iodide is the formerly reported $PrI_{2.42}$.

*To whom correspondence should be addressed.

0022-4596/91 $3.00

The metallothermic reduction of rare-earth halides with alkali metals, i.e., reactions like $MX_3 + A$, are an excellent tool for crystal growth in such reduced systems, because the alkali halides that are formed in the initial steps of the reduction reaction act as solvents. In many cases we have even obtained single crystals of metastable halides. Recently we have reported on the synthesis, crystal growth, and structure determination of Pr_2Br_5 (*5*), which is isostructural with Pr_2I_5 (*4*). La_2Br_5 (*6*), Ce_2Br_5 (*7*), and the analogous iodides (*8*) belong to the same structure type; the structures of the first two bromides have been refined from single-crystal X-ray data. During the course of this work the room-temperature crystal structure of Pr_2Br_5 has been reinvestigated from single-crystal X-ray data, and the low-temperature structures of Pr_2X_5 (X = Br, I) have been refined by powder neutron diffraction.

For some of the diiodides of the lanthanides, LnI_2 (Ln = La,Ce,Pr,Nd,Gd), metallic behavior had been suggested (*9–11*) and was later established (*12*) so that these halides should be formulated as, for example, $(La^{3+})(I^-)_2(e^-)$, designating their "free-electron" behavior. A similar formulation should be possible for Pr_2Br_5, i.e., $(Pr^{3+})_2(Br^-)_5(e^-)$. Preliminary bulk magnetic measurements on Pr_2X_5 (X = Br, I) had revealed very interesting magnetic properties with remarkably high ordering temperatures of 49 and 35 K, respectively. Further magnetic phase transitions at T = 20 K (Pr_2Br_5) and 9 K (Pr_2I_5) are indicated by second peaks in the magnetic susceptibility. The paramagnetic Curie temperatures $\Theta_p \approx 40$ K for both Pr_2Br_5 and Pr_2I_5 indicate substantial ferromagnetic interactions. It has been the aim of this work to establish the magnetic structures of the Pr_2X_5 halides (X = Br,I) and to acquire knowledge about their conductivity because a previous investigation (9) reports semiconducting behavior for such halides.

Experimental Details

Small single crystals of Pr_2Br_5 for X-ray structure determination are best obtained by metallothermic reduction of $PrBr_3$ with lithium. $PrBr_3$ was prepared via the ammonium halide route (*13*). A 1 : 1 molar mixture of $PrBr_3$ and Li was sealed under dry and anaerobic conditions in a tantalum tube by He-arc welding. The tube was then jacketed by a silica ampoule (for technical details see (*14*)), and heated to 560°C for 7 days. A few single crystals were selected in an Ar dry box, sealed into thin-walled glass capillaries, and checked for their quality, making use of single-crystal X-ray film techniques (rotation and Weissenberg). The best specimen was put on a Siemens AED 2 diffractometer. For details of the data collection and structure refinement processes see Table I.

The method of choice for the preparation of pure powder samples of Pr_2Br_5 and Pr_2I_5 in quantities sufficiently large for powder neutron diffraction is the conproportionation of PrX_3 (X = Br,I) and Pr metal (sublimed broken ingot). For the preparation of PrI_3, praseodymium metal powder that contains traces of hydrogen (better reaction kinetics) and iodine are reacted in a silica ampoule of 15 cm length and of an outer diameter of 1.8 cm under vacuum at 220°C for 1 day. The iodide is then purified by sublimation in a temperature gradient from 920 to 200°C. It is important to note that special care should be taken to ensure that even traces of water and oxygen are absent in the starting materials because they inevitably produce oxyhalides, $PrOX$.

A mixture of PrX_3 and Pr in a molar ratio of 5 to 1 was sealed into a carefully cleaned tantalum tube by He-arc welding and jacketed with silica as mentioned above. For the bromide and iodide alike, the reaction mixtures were heated for 3 days at 950°C, after which they were slowly cooled in the furnace to 550°C (Pr_2Br_5) and 650°C (Pr_2I_5), respectively. As the powders are especially sensitive to moisture (less to oxygen at am-

bient temperature), all manipulations were carried out in inert-gas dry boxes and the samples were inserted into gas-tight containers for all subsequent measurements.

Powder X-ray investigations were carried out with a Guinier camera (Simon technique, Enraf-Nonius, FR 553, Cu$K\alpha$ radiation) at ambient temperature and also between −170 and 700°C. All powder samples were checked and Guinier patterns could be indexed completely.

Neutron powder diffraction was carried out on the multidetector powder diffractometer DMC (*18*) and on the two-axis spectrometer 2AX of LNS at reactor Saphir of the Paul Scherrer Institut (Villigen, Switzerland) and later on diffractometers D1A and D2B at the Institut Laue–Langevin (Grenoble, France). In the case of the present low-symmetry magnetic structures, a particular advantage of D1A was the use of long-wavelength neutrons (λ = 299.9 pm) to resolve a maximum number of magnetic powder peaks. Such neutron diffraction measurements were performed at several temperatures on Pr_2X_5 (X = Br,I) and were the main basis for the refinement of magnetic ordering. For the neutron scattering experiments the powder samples were enclosed under pure He gas into cylindrical vanadium containers of a maximum height of 5 cm and diameter ϕ = 8 and 15 mm for DMC and D1A/D2B measurements, respectively. The profile intensities were corrected for absorption according to the measured transmission (μ = 0.154 and 0.216 cm^{-1} (λ = 170.6 pm) for X = Br, I, respectively). For the neutron diffraction investigations on diffractometers DMC and 2AX at reactor Saphir, and on D1A and D2B at ILL, the neutron wavelengths λ = 170.6, 233.7, 299.9, and 159.6 pm were used, respectively. The temperature dependences of selected magnetic Bragg peaks were measured on the two-axis diffractometer 2AX at reactor Saphir. Except for DMC investigations using a closed-cycle He refrigerator, low-temperature measurements were performed with "ILL-type" He gas flow cryostats.

Profile calculations for the refinements of the crystal and magnetic structures were carried out with the Young–Wiles (*19*) and a standard Rietveld program (*20*), respectively, using the neutron scattering lengths published by Sears (*21*) and a calculated relativistic neutron magnetic form factor of Pr^{3+} in the dipole approximation (*22*).

Electrical conductivity was measured by impedance spectroscopy making use of cylindrical pressed powder pellets (Pr_2Br_5: diameter 10 mm, height 4.65 mm, 83% of the X-ray density; Pr_2I_5: 10, 5.75, 92%). An impedance analyzer 4192A LF (Hewlett–Packard) was used for measurements between −60 and +100°C at frequencies ranging from 5 Hz to 13 MHz. The specimens reacted slowly with silver (Pr_2Br_5 above 75°C) and platinum contacts (Pr_2I_5 above 25°C) causing an increase in resistivity.

Results

The crystal structure of Pr_2Br_5 is as previously reported (*5*). The results of a more precise refinement from single-crystal X-ray diffraction data obtained at room temperature are summarized in Table I. There are no major differences from the results reported in 1987. Guinier patterns between −170 and 700°C showed no phase transition except for the melting of Pr_2Br_5 at 601°C (incongruent) and of Pr_2I_5 at 676°C (congruent).

The crystal and magnetic structures of Pr_2Br_5 and Pr_2I_5 are compared in Fig. 1. Note that the magnetic unit cells are outlined. Seven- (Pr1) and eight-coordinate (Pr2) praseodymium atoms are connected via $X2$ and $X3$ to double chains along [010] of the crystallographic unit cell (see Pr_2Br_5). The double chains form layers approximately parallel to (101), being connected by $X1$ and $X4$ between Pr1 and Pr2, respectively. These

TABLE I

Pr_2Br_5, CRYSTALLOGRAPHIC X-RAY DATA AT ROOM TEMPERATURE

Lattice constants (pm) (Guinier–Simon (a), single crystal (b) data):
(a) a = 778.76(8) b = 416.57(5) c = 1333.5(2) β = 90.993(8)°
(b) a = 778.7(3) b = 416.9(1) c = 1333.8(3) β = 91.04(5)°
Crystal system: monoclinic, space group $P2_1/m$, Z = 2.

Data collection and correction:
four-circle diffractometer Siemens–Stoe AED 2, Mo$K\alpha$-radiation, graphite monochromator, λ = 71.07 pm, ω-2θ-scan, scan speed variable, profile fit method (*15*), 1° < θ < 28°, $F(000)$ = 584, μ = 331.86 cm^{-1}, background, PL, and absorption corrections: ψ-scan for 20 reflections, $\Delta\psi$ = 10°.
Data statistics: 5506 reflections measured, 1202 unique (R_{int} = 5.4%).

Structure refinement
program system SHELX-76 (*16*), scattering factors from Cromer *et al.* (*17*), full-matrix least-squares refinement, R = 5.0%, R_w = 4,1%, w = 1.0016 $\sigma^{-2}(F_o)$.

Atomic positions and coefficients U_{ij}(pm^2) of the anisotropic temperature factors:

Atom	x/a	z/c	U_{11}	U_{22}	U_{33}	U_{13}
Pr1	0.4240(1)	0.65908(6)	172(4)	88(4)	135(4)	40(3)
Pr2	0.9264(1)	0.16170(6)	274(5)	74(4)	167(4)	91(4)
Br1	0.6924(2)	0.4892(1)	199(7)	135(8)	135(6)	35(6)
Br2	0.0443(2)	0.6767(1)	182(7)	167(8)	158(7)	31(6)
Br3	0.3481(2)	0.8787(1)	221(7)	186(8)	156(7)	39(6)
Br4	0.8493(2)	0.9305(1)	217(7)	132(8)	151(7)	44(6)
Br5	0.3318(2)	0.2718(1)	221(7)	120(8)	264(8)	−2(6)
		y/b = 0.25	$U_{23} = U_{12} = 0$			

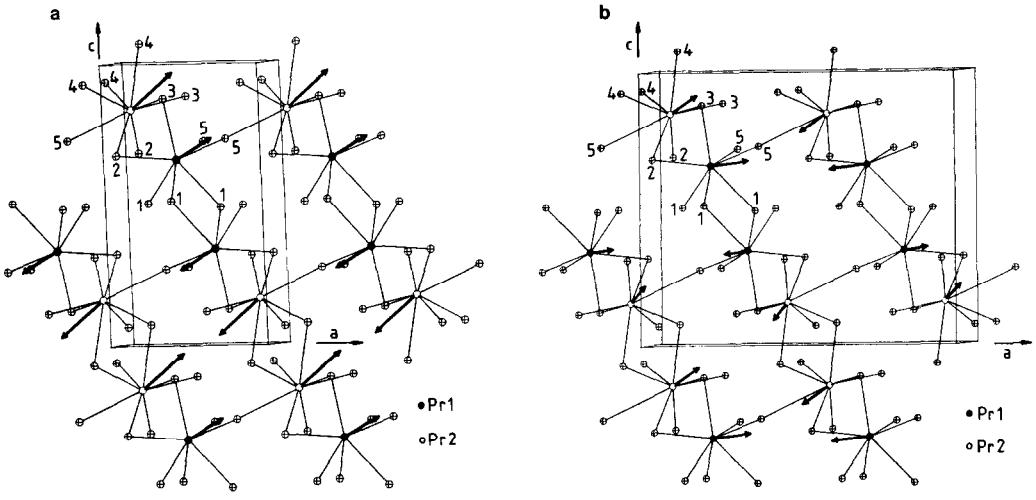

FIG. 1. Crystal and magnetic structures at 5 K of (a) Pr_2Br_5 and (b) Pr_2I_5. The magnetic unit cell is outlined.

TABLE II

CRYSTALLOGRAPHIC DATA FROM NEUTRON DIFFRACTION REFINEMENTS

(a) Pr_2Br_5 at 75 K (DMC, λ = 170.6 pm)
(b) Pr_2I_5 at 50 K (D2B, λ = 159.6 pm)

Lattice constants (pm):
(a) a = 774.60(6) b = 415.19(3) c = 1325.3(1) β = 91.066(5)°
(b) a = 863.35(3) b = 431.08(1) c = 1438.71(5) β = 89.458(2)°

Space group: $P2_1/m$, Z = 2

Atomic positions and isotropic temperature factors B(Å^2), y/b = 0.25 for all atoms:

	(a)			(b)		
Atom	x/a	z/c	B	x/a	z/c	B
Pr1	0.423(1)	0.6621(7)	0.3(2)	0.4157(6)	0.6600(3)	0.24(7)
Pr2	0.925(2)	0.1648(8)	0.9(2)	0.9025(6)	0.1544(3)	0.49(7)
X1	0.6936(9)	0.4900(5)	0.4(2)	0.6984(5)	0.4919(3)	0.36(8)
X2	0.0458(9)	0.6770(5)	0.3(1)	0.0492(5)	0.6828(3)	0.55(7)
X3	0.3519(9)	0.8784(5)	0.7(2)	0.3620(5)	0.8799(3)	0.44(7)
X4	0.8502(8)	0.9305(5)	0.7(2)	0.8520(5)	0.9264(3)	0.53(7)
X5	0.3303(8)	0.2713(5)	0.1(2)	0.3434(4)	0.2758(3)	0.20(7)
Reflections[a]	708			1241		
R_{wp}	5.0			5.1		
R_{exp}	1.9			2.2		
R_p	3.7			4.0		

[a] Number of inequivalent reflections used in calculation.

layers are connected to a three-dimensional structure over rather long bromide contacts: The room temperature distances Pr–Br5 are 295.7 (to Pr1) and 345.9 pm (to Pr2), respectively. The average Pr–Br distances are with 299.9 (Pr1, CN = 7) and 308.0 pm (Pr2, CN = 8), in good agreement with Pr^{3+}–Br^- distances for these coordination numbers known from K_2PrBr_5 (297.5 pm, CN = 7 (*23*)), attesting to a localized valence state of Pr^{3+} of $4f^2$ with one delocalized "free" electron per formula unit. Important for the understanding of the magnetic structure are the distances between the praseodymium nuclei. The shortest distances are 416.6 pm ($=b$) and 421.0 pm (Pr1–Pr2) for those located in the double chains.

Additionally, neutron powder diffraction patterns were recorded at different low temperatures down to 1.6 K. Structural parameters refined for paramagnetic Pr_2Br_5 at 75 K and for paramagnetic Pr_2I_5 at 50 K are summarized in Table II. Corresponding neutron diffraction patterns are shown in Fig. 2. Interatomic distances listed in Table III show an interesting anisotropic behavior. Lowering the temperature decreases the Pr–Br2 and Pr–Br3 distances, i.e., the distances in the Pr double chains, while the Pr1–Br1 and Pr2–Br4 distances increase. This separation of the layers toward double chains is also marked by the Pr–Pr distances. The Pr–Br5, i.e., the interlayer distances, slightly decrease upon cooling.

Pr_2I_5 exhibits a very similar behavior to Pr_2Br_5 in separating the layers toward double chains upon cooling, but with the difference that most Pr–I distances become smaller and the Pr–I5 distances increase. This increase of the interlayer distance is

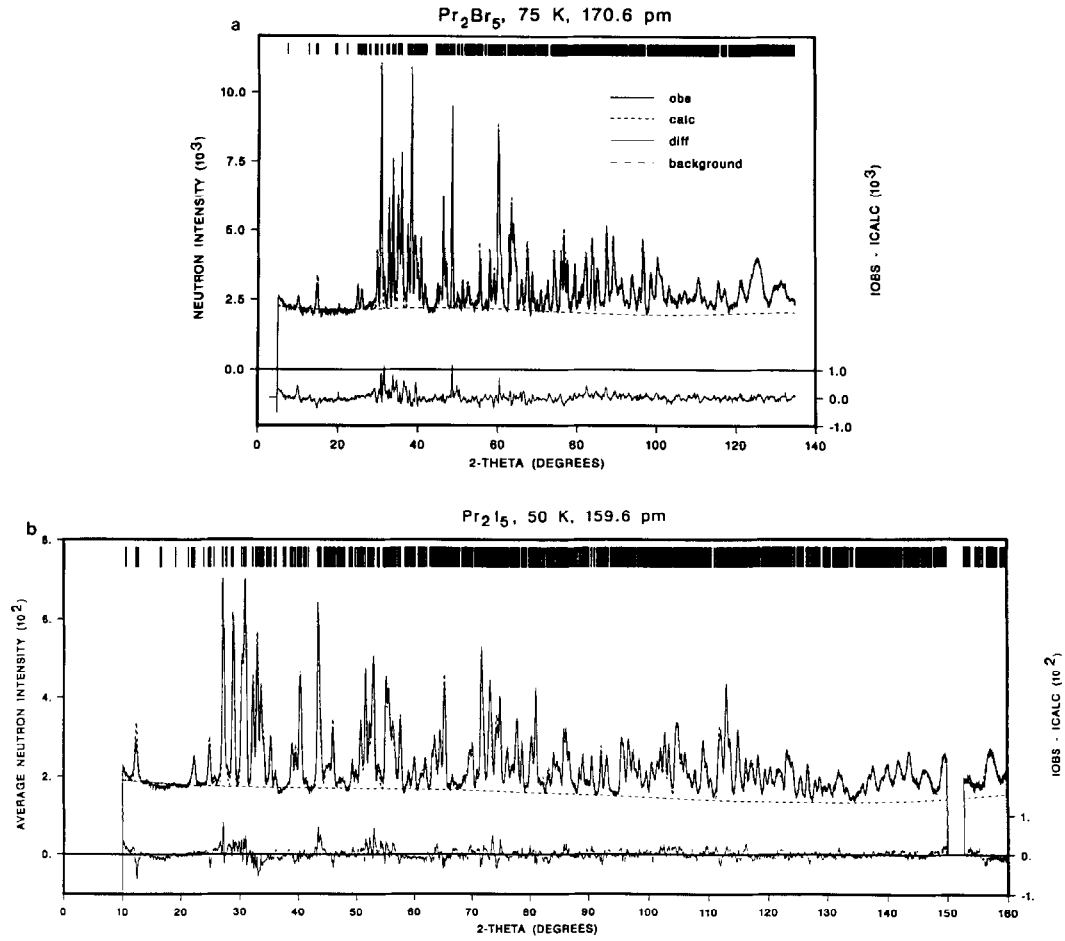

FIG. 2. Observed, calculated, and difference neutron diffraction patterns of (a) paramagnetic Pr_2Br_5 at $T = 75$ K (DMC measurement in the high-resolution mode) and (b) of paramagnetic Pr_2I_5 at $T = 50$ K (D2B measurement in the high-intensity mode). The origin of the weak temperature-independent peak in the Pr_2Br_5 diagram at $2\Theta \approx 9.7°$ could not be identified. The excluded region in the Pr_2I_5 diagram around $2\Theta \approx 150°$ is due to a cryostat Al peak.

probably due to the antiferromagnetic doubling of the *a*-axis.

Because of limitations in the sin Θ/λ range particularly in the $\lambda = 299.9$ pm measurements, the corresponding positional parameters were kept fixed in the low-temperature refinements of the magnetically ordered states (Table IV).

At lower temperatures, additional peaks resulting from long-range magnetic ordering occur in both cases. This is illustrated in Fig. 3. For Pr_2Br_5, these magnetic peaks may all be indexed on the basis of the "nuclear" unit cell, i.e., $\mathbf{k} = 0$. The intensity of the strongest magnetic peak (001) was followed in the temperature range of 60 to 1.6 K. Figure 4a shows that two magnetic ordering phenomena start at 50 and 25 K, respectively, which is in approximate agreement with bulk magnetic measure-

TABLE III

IMPORTANT DISTANCES (pm) IN Pr_2Br_5 AND Pr_2I_5

(a) Pr_2Br_5 X-ray data at 25°C
(b) Pr_2Br_5 neutron diffraction data at 75 K (DMC, λ = 170.6 pm)
(c) Pr_2I_5 X-ray data at 25°C calculated from (*4*)
(d) Pr_2I_5 neutron diffraction data at 50 K (D2B, λ = 159.6 pm)

	Mult.	(a)	(b)	(c)	(d)
Pr1–Pr1 (=b)	2	416.57(5)	415.19(3)	431.7(8)	431.08(1)
(intralayer)	2	489.0(1)	494(2)	523.7(2)	527.6(6)
Pr1–Pr2	2	421.0(1)	413(1)	451.8(2)	438.0(6)
(interlayer)	2	593.5(1)	589(2)	671.0(2)	683.5(7)
Pr2–Pr2 (=b)	2	416.57(5)	415.19(3)	431.7(8)	431.08(1)
(intralayer)	2	494.2(1)	499(2)	517.8(2)	520.4(6)
Pr1–X1	2	300.1(1)	302.0(8)	325.4(1)	323.0(5)
	1	310.9(2)	313(1)	347.2(2)	342.0(6)
Pr1–X2	1	297.0(2)	293(1)	320.2(2)	317.8(7)
Pr1–X3	1	299.8(2)	293(1)	323.3(2)	319.3(6)
Pr1–X5	2	295.7(1)	294.6(8)	306.3(1)	314.0(5)
Pr2–X2	2	300.3(1)	295.6(9)	320.5(1)	321.3(5)
Pr2–X3	2	302.6(1)	303(1)	331.3(2)	318.2(5)
Pr2–X4	2	299.6(1)	300.5(9)	313.2(2)	323.2(5)
	1	313.0(2)	315(1)	334.4(2)	331.3(6)
Pr2–X5	1	345.9(2)	342(1)	418.0(2)	420.3(6)
$\bar{d}$(Pr1–X)	7	299.9	298.9	322.0	321.9
$\bar{d}$(Pr2–X)	8	308.0	306.9	335.3	334.6

ments. Further neutron diffraction patterns were therefore recorded at 30 and 5 K (D1A) and 1.6 K (DMC), i.e., at the plateaus of the intensity vs temperature curve for the magnetic peak (001). The best fit of the observed and calculated intensities was obtained for the Shubnikov space group $P2_1/m'$ (*24*) (Figs. 3b and 3c). As all praseodymium atoms occupy the special position (2*e*): x, 1/4, z and, therefore, lie on a mirror plane m' parallel (010), coupling of the magnetic moments as axial vectors is only possible in this plane and has to be antiferromagnetic according to the magnetic moment components (μ_x, 0, μ_z) at position (x, 1/4, z) and ($-\mu_x$, 0, $-\mu_z$) at site ($-x$, 3/4, $-z$). The calculated magnetic moments are summarized in Table IV and their directions are shown in Fig. 1. The second ordering phenomenon, typically at 1.6 K, is different from that at, for example, 30 K in that the magnetic moments increase from μ_{Pr1} = 1.2 μ_B and μ_{Pr2} = 2.2 μ_B at T = 30 K to μ_{Pr1} = 1.9 μ_B and μ_{Pr2} = 2.6 μ_B at T = 5 K, different for both praseodymium sites; see Table IV.

In contrast to Pr_2Br_5, magnetic Bragg peaks that cannot be indexed with the crystallographic unit cell occur in the neutron powder diffraction pattern for Pr_2I_5 below 37 K. However, indexing is possible by doubling the a-axis. Then all magnetic peaks have odd h indices, implying antiferromagnetic coupling along [100]. Therefore, the magnetic unit cell results from the "nuclear" one with an antitranslation in the [100] direction. The Shubnikov group P_a2_1 yields the best results, e.g., Fig. 3e. The coupling scheme is as follows (y = 1/4 and written for P_a2_1'):

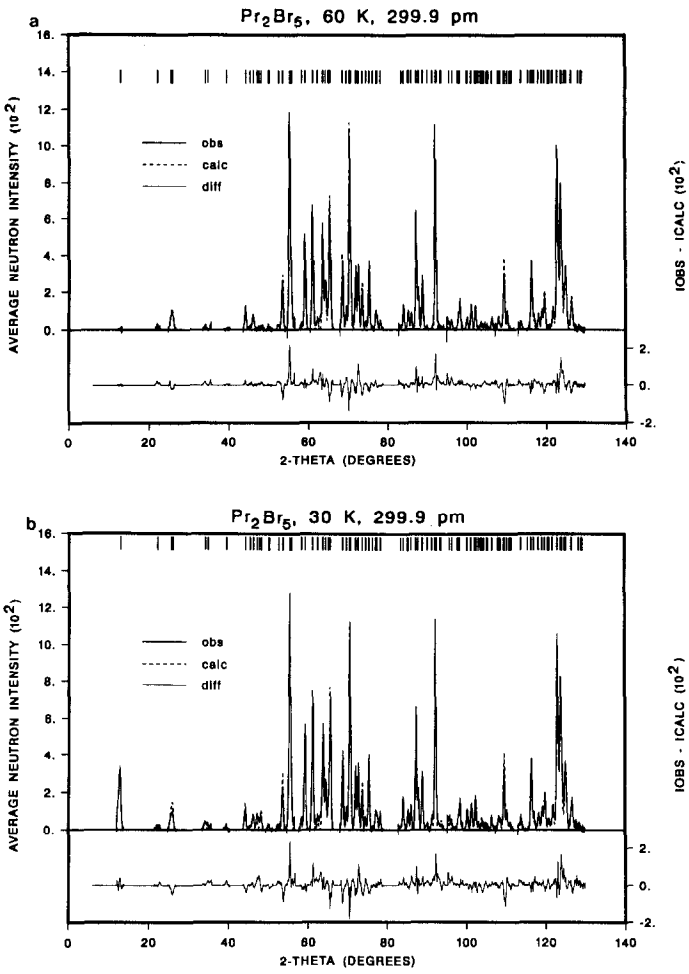

FIG. 3. Observed (background subtracted), calculated, and difference neutron diffraction patterns (D1A measurements) of (a) paramagnetic Pr_2Br_5 at $T = 60$ K, magnetically ordered Pr_2Br_5 at (b) $T = 30$ K and (c) $T = 5$ K, (d) paramagnetic Pr_2I_5 at $T = 50$ K, and (e) antiferromagnetic Pr_2I_5 at $T = 5$ K. In the latter case the upper and lower vertical bars at the top of the figure show the 2Θ positions of magnetic and nuclear Bragg peaks, respectively.

(x, y, z) $(1/2+x, y, z)$
(μ_x, μ_y, μ_z) $(-\mu_x, -\mu_y, -\mu_z)$

$(-x, 1/2+y, -z)$ $(1/2-x, 1/2+y, -z)$
$(\mu_x, -\mu_y, \mu_z)$ $(-\mu_x, \mu_y, -\mu_z)$.

For better comparison with the paramagnetic structure, the nonconvenient magnetic space group P_a2_1' is chosen. It can be transformed to P_a2_1 by an origin shift of (1/4, 0, 0). The only important differences from the coupling scheme for Pr_2Br_5 are that in Pr_2I_5 magnetic moment components in the [010] direction become possible subject to the absence of the mirror plane parallel to (010) and the directions of the magnetic moments are inverted in every other chemical cell because of the antidoubling of the a-axis. Further results are summarized in Table IV.

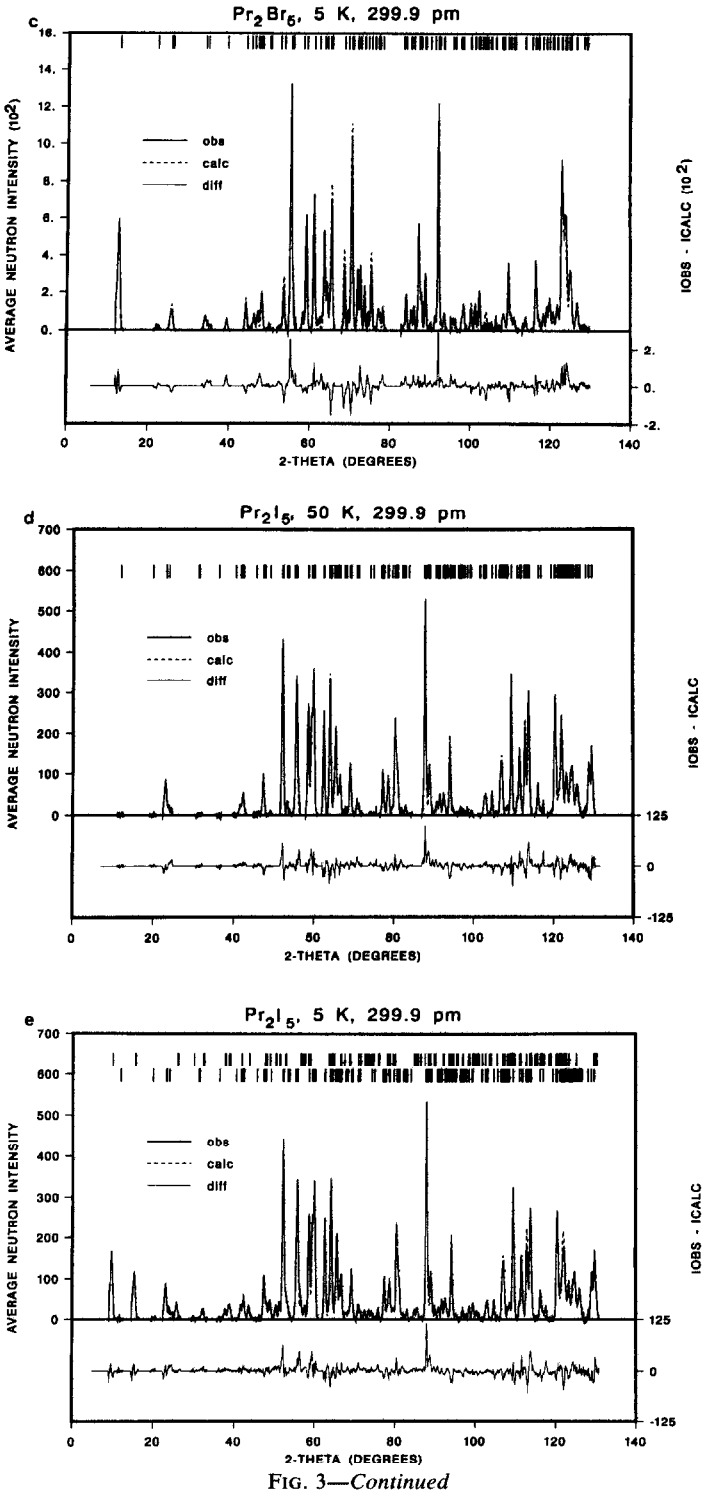

FIG. 3—*Continued*

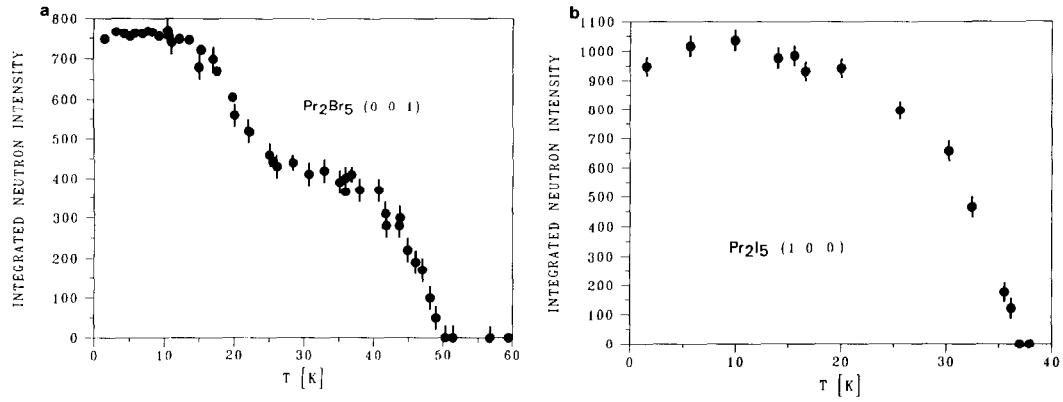

FIG. 4. Temperature dependences of selected magnetic Bragg peaks of (a) Pr_2Br_5 and (b) Pr_2I_5. Note the magnetic phase transition in case of Pr_2Br_5 at $T \approx 25$ K.

The temperature dependence of the magnetic Bragg peak (100) as shown in Fig. 4b does not indicate the second magnetic phase transition around 9 K which was observed in bulk magnetic investigations within error limits.

Conductivity measurements show that both halides are "within the powder average" semiconductors with specific conductivities of $2.6 \times 10^{-4}/(\Omega \cdot \text{cm})$ at 22.5°C (Pr_2Br_5) and $6.4 \times 10^{-4}/(\Omega \cdot \text{cm})$ at 25.0°C (Pr_2I_5) (see Fig. 5). Reaction between the samples and the cell contacts above 25°C (Pr_2Br_5) and 75°C (Pr_2I_5) causes a decreasing conductivity in the upper temperature range.

In contrast to conductivity measurements, extended-Hückel molecular orbital calculations on Pr_2Br_5 show a *d*-block splitting for Pr with two very narrow bands at lower energy. These bands are folded along the *b*-axis and half-filled with two electrons. Due to this situation, metallic behavior should be expected unless electrons are localized. Interactions between the widely spaced Pr atoms appear to be rather weak, as evaluated from the crystal orbital overlap populations (COOP), with interactions between Pr1–Pr1 along [010] and the short Pr1–Pr2 (421.0 pm) contact (*26*).

Discussion

The results as reported above show clearly that both Pr_2Br_5 and Pr_2I_5 are halides in which prascodymium is trivalent in a sense that a localized $4f^2$ valence state is present with one "free" electron per formula unit. This delocalized electron must be responsible for the high magnetic ordering temperatures of 50 K in Pr_2Br_5 and 37 K in Pr_2I_5, respectively.

A comparably high ordering temperature of 41 K has been observed for Tb_2Cl_3 (*25*). As Pr_2Br_5 contains Pr^{3+}, Tb_2Cl_3 contains Tb^{3+}, but terbium forms octahedral $[Tb_6]$ clusters connected via common edges to infinite chains.

The remarkable second magnetic phase transition at $T \approx 25$ K in Pr_2Br_5 can be attributed to different temperature dependences of the magnetic moments of the two inequivalent praseodymium sites, presumably caused by the different coordination and, associated therewith, crystal field and magnetic interaction effects. Also, the directions of the magnetic moments are different in the two ordering regions. The onset of the two ordering temperatures is also observed in bulk magnetic (susceptibility) measurements. This is seen in such measurements

TABLE IV

RESULTS OF NEUTRON DIFFRACTION REFINEMENTS ON MAGNETICALLY ORDERED Pr_2Br_5 AND Pr_2I_5 (AXES (pm), β(°), B(Å^2), R(%), $\mu(\mu_B)$) D1A, λ = 299.9 pm

	Pr_2Br_5			Pr_2I_5	
	60 K	30 K	5 K	50 K	5 K
a	776.82(8)	775.96(5)	775.78(5)	864.74(8)	1729.75(9)
b	416.42(5)	416.25(3)	416.37(3)	431.70(4)	431.74(2)
c	1329.0(1)	1327.61(9)	1327.2(1)	1440.5(1)	1439.94(7)
β	91.074(2)	91.103(3)	91.113(4)	89.469(2)	89.455(2)
B_{Pr}	0	0	0	0.2(2)	0.2
B_X	0.30(9)	0.3	0.3	0.14(9)	0.14
Refl.	132	132	132	162	330
R_{wp}	19.2	21.4	22.3	16.8	17.7
R_{exp}	5.6	6.2	5.6	7.0	7.9
R_{IN}	14.3	14.3	15.6	10.7	10.5
R_{IM}	—	22.8	18.9	—	16.1
μ_{Pr1}		1.2(2)	1.9(3)		2.14(9)
μ_x		1.1(2)	1.6(4)		1.54(8)
μ_y		—	—		1.47(6)
μ_z		0.5(1)	0.9(2)		0.2(1)
μ_{Pr2}		2.2(2)	2.6(2)		1.8(1)
μ_x		−1.6(2)	−2.0(4)		−1.04(7)
μ_y		—	—		1.18(9)
μ_z		−1.5(1)	−1.6(2)		−0.88(8)

for Pr_2I_5, too. However, only a single magnetic phase transition was observed from neutron diffraction data.

Despite the similarities of the crystal structures of Pr_2Br_5 and Pr_2I_5 as illustrated in Fig. 1 the magnetic structures are different: They correspond to $\mathbf{k}$ = 0 and [1/2, 0, 0], respectively. Based on the neutron diffraction results these magnetic ordering effects appear to be antiferromagnetic (Pr1–Pr1, Pr2–Pr2). Except for this, the interaction between the different Pr sites (Pr1–Pr2) is predominantly ferromagnetic, causing the positive paramagnetic Curie temperature $\Theta_p \approx 40$ K calculated for both compounds from magnetic susceptibility measurements. Θ is determined by nearest-neighbor interactions, of which the Pr1–Pr2 interaction and the Pr1–Pr1 and Pr2–Pr2 interactions along the short b-axis must be dominant because Θ is positive. This is also reflected by the shortest Pr–Pr distances (see Table III) which are equal within a few picometers. These short connections must provide the most efficient exchange pathway. The resulting magnetic structure (see Fig. 1) thus consists of predominantly ferromagnetically coupled double chains, which order antiferromagnetically at low temperatures as the result of a weak antiferromagnetic interchain interaction. Presumably due to crystal field effects, the ordered magnetic moments of Pr1 and Pr2 in Pr_2X_5 at saturation appear to be significantly reduced below the value $g \cdot J = 3.20$ of Pr^{3+} for the $^3H_4$ ground state: $\mu_{Pr1} = 1.9\ \mu_B$ and $\mu_{Pr2} = 2.6\ \mu_B$ for the bromide and $\mu_{Pr1} = 2.1\ \mu_B$, $\mu_{Pr2} = 1.8\ \mu_B$ for the iodide.

Another surprising result is that the "free-electron" Pr_2X_5 type halides seem to be semiconductors "in the powder average." That the free electron cannot be localized in

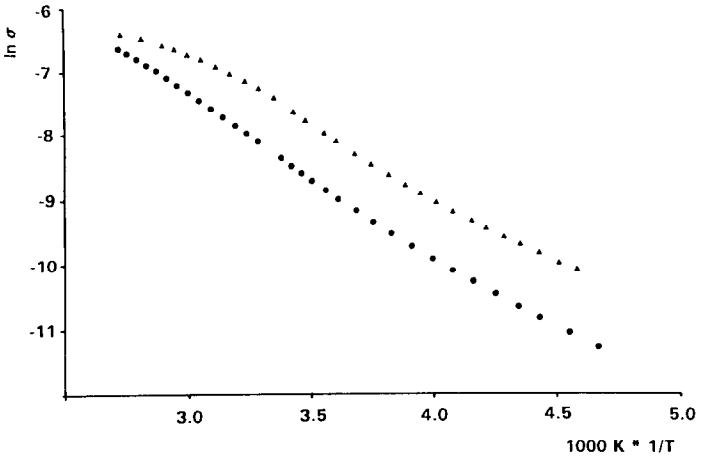

FIG. 5. Reciprocal temperature dependence of the logarithmic conductivity of Pr_2Br_5 (circles) and Pr_2I_5 (triangles).

a sense that a mixed valence compound with di- and trivalent praseodymium would occur, is also clear from X-ray absorption near edge spectroscopy (XANES) which only shows one peak which by comparison with, for example, $PrBr_3$, can doubtlessly be attributed to Pr^{3+} with the electronic configuration $4f^2$. Calculations of the electronic structure of Pr_2Br_5 (*26*) using the extended Hückel method initially seemed to contradict the experimentally obtained weak semiconducting behavior. The band structure shows two narrow *d* bands containing two electrons, split off more than 1 eV below the Pr *d*-block. This should lead to metallic conductivity, consistent with the formulation $(Pr^{3+})_2(Br^-)_5(e^-)$, unless the electrons are localized. The band structure, however, is rather distinct from a metal like LaI_2 (*12*), because for the two narrow (half-filled) bands in Pr_2Br_5 electron–electron interactions become important, such as on-site electron repulsion. Thus electrons were considered to be localized on lattice sites in terms of Mott insulating states.

Acknowledgments

This work has been largely supported by the Deutsche Forschungsgemeinschaft, Bonn, and by the Fonds der Chemischen Industrie, Frankfurt/Main. We are also grateful to Prof. W. Bronger, Aachen, to Prof. D. Johnston and Dr. L. Miller, Ames, Iowa, to Dr. N. Edelstein, Berkeley, California, for susceptibility measurements, and to Prof. G. Kaindl, Berlin, for XANES data on which we report separately with investigations on analogous compounds. Furthermore, we thank Dr. H.-J. Meyer, Hannover, for extended-Hückel calculations and Prof. A. Furrer, LNS, for stimulating discussions and preliminary crystal field measurements on Pr_2X_5. For general support of the present investigations we are indebted to LNS, PSI, and ILL.

References

1. L. F. DRUDING, J. D. CORBETT, AND B. N. RAMSEY, *Inorg. Chem.* **2,** 867 (1963).
2. R. A. SALLACH AND J. D. CORBETT, *Inorg. Chem.* **2,** 457 (1963).
3. J. D. CORBETT, L. F. DRUDING, W. J. BURKHARD, AND C. B. LINDAHL, *Discuss. Faraday Soc.* **32,** 79 (1961).
4. E. WARKENTIN, Dissertation, Karlsruhe, F.R.G. 1977.
5. TH. SCHLEID AND G. MEYER, *Z. Anorg. Allg. Chem.* **552,** 97 (1987).
6. K. KRÄMER, TH. SCHLEID, M. SCHULZE, W. URLAND, AND G. MEYER, *Z. Anorg. Allg. Chem.* **575,** 61 (1989).
7. K. KRÄMER AND G. MEYER, *Eur. J. Solid State Inorg. Chem.* **28,** 523 (1991).
8. "Gmelin Handbuch der Anorganischen Chemie," Syst.-Nr. 39, C6, p. 153, Springer-Verlag, Berlin/Heidelberg/New York (1978).

9. J. D. CORBETT, R. A. SALLACH, AND D. A. LOKKEN, *Adv. Chem.* **71,** 56 (1967).
10. J. D. CORBETT, *Inorg. Chem.* **22,** 2669 (1983).
11. H. J. MATTAUSCH, A. SIMON, N. HOLZER, AND R. EGER, *Z. Anorg. Allg. Chem.* **466,** 7 (1980).
12. J. H. BURROW, C. H. MAULE, P. STRANGE, J. N. TOTHILL, AND J. A. WILSON, *J. Phys. C Solid State Phys.* **20,** 4115 (1987).
13. G. MEYER, S. DÖTSCH, AND TH. STAFFEL, *J. Less-Common Met.* **127,** 155 (1987).
14. J. D. CORBETT, *Inorg. Synth.* **22,** 15 (1983).
15. W. CLEGG, *Acta Crystallogr. Sect. A* **37,** 22 (1981).
16. G. M. SHELDRICK, "SHELX-76: Program for Crystal Structure Determination," Cambridge, U.K. (1976).
17. D. T. CROMER AND J. B. MANN, *Acta Crystallogr. Sect. A* **24,** 321 (1968). D. T. CROMER AND D. LIBERMANN, *J. Chem. Phys.* **53,** 1891 (1970).
18. J. SCHEFER, P. FISCHER, H. HEER, A. ISACSON, M. KOCH, AND R. THUT, *Nucl. Instr. Methods Phys. Res. A* **288,** 477 (1990).
19. D. B. WILES AND R. A. YOUNG, *J. Appl. Crystallogr.* **14,** 149 (1981); ILL/LNS program version modified by I. Rodriguez, P. Fischer, and J. Schefer.
20. H. M. RIETVELD, *J. Appl. Crystallogr.* **2,** 65 (1969); A. W. HEWAT, Harwell report AERE-R7350 (1973); J. C. HOWARD, *J. Appl. Crystallogr.* **15,** 615 (1981).
21. V. F. SEARS, "Methods of Experimental Physics" (K. Sköld and D. L. Price, Eds.), Vol. 23A, p. 599, Academic Press, London (1986).
22. A. J. FREEMAN AND J. P. DESCLAUX, *J. Magn. Magn. Mater.* **12,** 11 (1979).
23. G. MEYER, J. SOOSE, A. MORITZ, V. VITT, AND TH. HOLLJES, *Z. Anorg. Allg. Chem.* **521,** 161 (1985).
24. W. OPECHOWSKI AND R. GUCCIONE, "Magnetism" (G. T. Rado and H. Suhl, Eds.), Vol. II, Part A, Academic Press, New York/London (1965).
25. B. SCHMID, P. FISCHER, R. KREMER, A. SIMON, AND A. W. HEWAT, *J. Phys.* **49,** C8-841 (1988).
26. H. J. MEYER AND R. HOFFMANN, *J. Solid State Chem.*, **95,** 14 (1991).